Hindawi
International Journal of Photoenergy
Volume 2019, Article ID 6808347, 10 pages
https://doi.org/10.1155/2019/6808347

Research Article

Electrochemical Coprecipitation of Zinc and Aluminum in Aqueous Electrolytes for ZnO and AZO Coverage Deposition

Natalia A. Martynova,[1] Viktor N. Svishchev,[1] Leonid S. Lepnev,[2] Shakhnozabonu R. Alieva,[1] Elena G. Chertorylskaya,[3] Mikhail E. Vishnevskiy,[3] Alexey D. Bozhko,[4] and Anastasia V. Grigorieva[1]

[1]*Lomonosov Moscow State University, Leninskie gory 1/73, 119991 Moscow, Russia*
[2]*Lebedev Physical Institute of the Russian Academy of Sciences, Leninskiy Prospect 53, 119991 Moscow, Russia*
[3]*ZAO "SPECS", Leninskiy Prospect 31, 119991 Moscow, Russia*
[4]*Prokhorov General Physics Institute of the Russian Academy of Sciences, Vavilov str. 38, 119991 Moscow, Russia*

Correspondence should be addressed to Anastasia V. Grigorieva; anastasia.grigorieva@gmail.com

Received 1 February 2019; Accepted 2 April 2019; Published 7 May 2019

Guest Editor: Chunling Wang

The aim of this study is to examine the technological challenge of the electrochemical formation of zinc oxide and Al-doped ZnO films (ZnO:Al, AZO) as transparent conductive oxide coatings with complex architectures for solar cell photoanode materials. A cathodic electrodeposition of AZO was performed using aqueous nitrate electrolytes at 25°C. A significant positive deviation in aluminum percentage in the films was demonstrated by the LAES, EDX, and XPS methods, which originates from aluminum hydroxide sedimentation. The photoluminescent characteristics of the ZnO films reveal low band intensities related to intrinsic defects, while the samples with 1 at.% of aluminum show a strong and wide PL band at 600 ± 80 nm and increase in conductivity.

1. Introduction

Zinc oxide (ZnO) is a multifunctional material, mostly due to its transparent and conducting characteristics and its advantages in a wide range of technological applications such as electrodes in solar cells and in flat-panel displays, touch control panels, shields with electromagnetic protection, light-emitting diodes (LEDs), and smart windows. In order to improve the electrical and optical properties of transparent semiconductive ZnO films, oxide was doped with a number of metal or nonmetal elements. Aluminum-doped ZnO films (AZO) are considered the most promising alternative to expensive indium-based ITO for transparent conducting oxide materials for solar cells.

AZO thin films can be prepared by various techniques such as sol-gel synthesis [1–3], atomic layer deposition [4–6], chemical pyrolysis [7], chemical vapor deposition (CVD) [8], magnetron sputtering [9, 10], and pulsed laser deposition [11]. Most of these methods require a controlled environment, which makes the processing complicated and expensive. One of the promising methods for film deposition is electrochemical deposition. The technique is simple and cost-effective and is a single-step preparation. Electrodeposition offers unique features such as scalability, easiness of implementation, and accurate control of film thickness and morphology. Electroplating is a simple and easy-scaling method for the production of metal oxide films with different morphological shapes. In addition, the electrodeposition method has several benefits such as low cost, material efficiency, and energy efficiency and is a standard technique worldwide. Furthermore, the preparation of AZO thin films by electrocrystallization can be environmentally safe, and nontoxic chemicals can be used in electrolytic baths.

It should be noted that only very few articles describe the electrochemical deposition of zinc and aluminum oxide. Most of these electrochemical approaches reported for ZnO film preparation use an aqueous bath of zinc salt such as zinc chloride and zinc nitrate, with the commonly used zinc

precursors in zinc electrolytic baths [12]. Additionally, oxygen precursors like nitrates (NO^{3-}) and molecular oxygen (O_2) dissolved in water or hydrogen peroxide (H_2O_2) [13] should be applied to reach metal zinc oxidation. Regardless of the oxygen precursors applied, crystalline ZnO thin films with optical transparency can be obtained. According to [10], a higher Hall mobility can be expected for films with an increased grain size and Al concentration of 2 at.%. The corresponding optical bandgap values for such films reach 3.8 eV increasing from 3.4 eV, while the transmittance is 85%.

Most publications on the deposition of ZnO from zinc nitrate baths describe a uniform film growth for heating up to 80°C only when individual ZnO particles are round-shaped or hexagon-like, depending on deposition conditions. According to Refs. [14, 15], polycrystalline ZnO films could be grown up successfully in aqueous nitrate electrolytes.

In Ref. [16], authors report the electrodeposition of AZO using zinc-aluminum nitrate electrolytes. For electrolytes with Al^{3+} concentrations up to 0.3 mM, the formation of a top-layer amorphous Al_2O_3 is observed. For the films obtained, EIS measurements confirm their n-type character and also an increase in the charge carrier density (ND) from 10^{19} to 10^{20} cm^{-3} as Al is incorporated. The optical band gap increases with the Al content from 2.8 eV for undoped ZnO up to 3.45 eV for ZnO:Al with 11 at% Al. The blue shift of the band gap values is consistent with the Burstein-Moss effect. The Urbach tail parameter analysis suggests that electronic defects from Al doping cause to extend the optical absorption responsible for the observed photocurrent increase. Film transparencies up to 60% at 550 nm and a carrier density in the order of the ITO substrate suggest that films with 11% at Al content could be suitable as transparent conductive oxide in thin film solar cells. So both publications [10, 16] demonstrate the evolution of optical properties that, most likely, originates from some changes in the surface composition of coatings with various aluminum percentages. The surface composition of AZO coatings is also of great importance for its further application in electrical setups.

In this article, electrocrystallization of zinc oxide at ITO substrates was carried out using nitrate electrolytic baths with $Zn(NO_3)_2$ as a zinc precursor and aluminum nitrate as a source of Al^{3+} ions. The chemical composition of zinc and aluminum coprecipitation products obtained in an electrical field at room temperature (RT) was analyzed precisely to reveal any admixture phases. The effect of the aluminum percentage on the optical and electrical properties of AZO was assessed through UV–vis optical transmittance, photoluminescent spectroscopy, and two-fold electrical measurements.

2. Experimental

Al-doped ZnO films have been prepared by mutual electrochemical deposition of zinc and zinc oxide. The process has been carried out in a three-electrode cell at room temperature from nitrate aqueous baths. The zinc bath composition included just nitrates, namely, 0.2 M $Zn(NO_3)_2$, 0.5 M KNO_3, and 0.0032 M $Al(NO_3)_3$. The working and counter electrodes have been placed parallel to each other and separated by 2 cm. The reference electrode is a saturated aqueous Ag/AgCl/KCl(s) electrode connected to the cell via a Luggin capillary. A platinum wire of 0.5 mm diameter has been applied as a counter electrode. The samples with a different theoretical thickness of $h = 300 - 2000$ nm have been prepared. The amount of the precipitated metal and, consequently, film thickness h, is estimated using Faraday law from the deposition charge under the assumption of 100% current efficiency. Cyclic voltammetry (CV) has been carried out in the range of -2.5 – 0 V vs. Ag/AgCl/KCl(s) electrode.

The sample morphologies of ZnO films are examined using a Leo Supra 50 VP scanning electron microscope or a Carl Zeiss NVision 40 scanning electron microscope (SEM). Both the instruments are equipped with EDX Oxford Instruments attachments for the local chemical analysis.

TG-DTA analysis has been performed with preliminary delaminated pristine coatings of complex composition. All measurements have been carried out using STA 409 PC Luxx coupled with a quadrupole mass spectrometer QMS 403C Aëolos (NETZSCH). Annealing has been done in argon as a gas carrier with a flow rate of 30 ml/min. The samples have been annealed up to 800°C with a heating rate of 5°/min and an isotherm at 800°C for 30 min.

Mass spectrometry with inductively coupled plasma (ICP MS) analyses of electrolyte contents have been carried out using an ICP spectrometer Perkin-Elmer ELAN DRC-II. Standard solutions have been prepared to correspond to a range of concentrations of the components to be determined at 0-10 μg/l. Standard aliquots of zinc and aluminum ions with concentrations of 1 mg/cm^3 have been used for constructing the calibration graph. Electrolytes with theoretical mole fractions of aluminum of 1, 2, 4, 6, and 10 at.% have been specified. Two additional series of probes have been prepared from the initial electrolytes. In the first series electrolytes have been diluted $6 \cdot 10^6$ times, while in the second series the dilution has been done $3.6 \cdot 10^7$, in order to reach the concentration of ions (Al and Zn) in the range 0-10 mcg/l.

Laser atomic emission spectroscopy (LAES) has been carried out for semiquantitative analysis of aluminum percentage in the films deposited. The spectral recording system is implemented on a monochromator-spectrograph with a 4-position turret of replaceable diffraction gratings and a CCD detector from Toshiba or on several Paschen-Runge-type polychromators with five Toshiba CCD linear detectors with the following characteristics: range of wavelengths 177-800 nm, reproducibility ±0.01 nm, spectral resolution < 0.012 nm, accuracy of setting the wavelength ± 0.01 nm. The scanning mode was as follows: defocusing—2 times, energy—13 J, the number of pulses per point—3, and the number of points ("shots")—5-9.

The XPS spectra have been recorded on a laboratory spectrometer PHI5500VersaProbeII. The excitation source is monochromatized Al Kα radiation (hν = 1486.6 eV), and power is 50 W. The analysis area is 200 μm in diameter. Use of a neutralizer-double neutralization (electronic and ionic) is used. The elemental analysis was as follows: atomic concentrations are determined from overview spectra by the method of factors of relative element sensitivity by the

lines C1s, O1s, Zn2p3, N1s, Al2p, Cl2p, K2p, and In3d5. High-resolution spectra are recorded at transmission energy of the analyzer of 23.5 eV and a data acquisition density of 0.2 eV/step.

The dark DC electrical resistivity of the films studied has been measured at room temperature by a routine 2-terminal technique in a capacitor configuration. The contacts to the films and to the substrate were prepared using Ag paint.

3. Results and Discussion

3.1. Voltammograms and Deposition. Experiments on the deposition of Al-doped zinc oxide were carried out using conductive transparent ITO substrates to examine the microstructure and composition for further application as photoanodes. The corresponding cyclic voltammetry (CV) curves and preferred electroplating modes are presented in Figure 1 and Table 1.

According to CV data and other studies [17], the growth mechanism of ZnO films from nitrate electrolytes can be described by the following processes. The first one is the reduction of nitrate ions, which produces nitrite and hydroxide ions at the cathode. This is followed by the interaction of zinc cations Zn^{2+} with hydroxide ions, forming zinc hydroxide. After dehydration of the hydroxide, ZnO is formed as a final product. The mechanism of ZnO electrodeposition in the nitrate electrolyte is described by equations (1), (2), (3), and (4):

$$Zn(NO_3)_2 \rightarrow Zn^{2+} + 2NO_3{}^- \quad (1)$$

$$NO_3{}^- + H_2O + 2e^- \rightarrow NO_2{}^- + 2OH^- \quad (2)$$

The reduction of nitrate ions (NO^{3-}) to nitrite ions and release of hydroxyl ions (OH^-) occur at about −0.70 V vs. Ag/AgCl/KCl(s). The formation of $Zn(OH)_2$ or ZnO deposits occurs according to equations (3) and (4). When the applied potential is around −0.75 V, hydroxyl ions OH^- generated at the cathode produce $Zn(OH)_2$ which turns to zinc oxide ZnO.

$$Zn^{2+} + 2OH^- \rightarrow Zn(OH)_2 \quad (3)$$

$$Zn(OH)_2 \rightarrow ZnO + H_2O \quad (4)$$

Reduction of Zn^{2+} ions to metallic zinc occurs below −1.0 V:

$$Zn^{2+} + 2e^- \rightarrow Zn_{(s)} \quad (5)$$

This deposition mechanism indicates that zinc hydroxide $Zn(OH)_2$ is an appropriate precursor for ZnO electrochemical growth because of its slower deposition rate and easy zincite formation on heating. The formation of zinc hydroxide is optimal for controlling the morphology of the product, including nucleation processes and growth and phase boundary formation between the ZnO grains. On the other hand, slow electrocrystallization of metal zinc with the subsequent oxidation is an alternative way to obtaining a uniform transparent coating. The formation of zincite-like ZnO occurs right at the cathode if the concentration of hydroxyl ions is low. The growth kinetics and also habitus of the crystallites is mostly determined by the concentration of Zn^{2+} ions in the near-cathode region.

In order to identify the electrodeposition processes and to verify the electrochemical behavior of the electrodes in nitrate baths, cyclic voltammetry measurements were carried out. Figure 1 shows the cyclic voltammograms recorded at 25°C in the potential range from 0 to −2.5 V vs. Ag/AgCl/KCl(s) in nitrate baths. An increase in the cathodic current density begins at about 0.85 V, which corresponds to the nitrate ion reduction (equation (2)). The next increase at around -1.1 V corresponds to the reduction of zinc ion Zn^{2+} into metallic zinc. During the reverse anodic scan, no anodic currents are observed, which points to the high stability of the films without any delamination processes. In order to understand the impact of Al^{3+} during the reduction process, voltamperometry was performed for the baths with different concentrations of $Al(NO_3)_3$ (from 0 to 0.0256 M) and with a constant $Zn(NO_3)_2$ concentration of 0.2 M. Figure 1(b) demonstrates that CV curves for electrolytes consisted only of $Al(NO_3)_3$ or $Zn(NO_3)_2$ in order to determine the optimal deposition potentials for Al and Zn independently. For mixed zinc and aluminum electrolytes, the deposition potential of -1.1 V was applied to effectively deposit both kinds of cations. The average deposition rate for the samples obtained at different potentials in the range of (-1.3 – -1.1 V) vs. Ag/AgCl was insignificant. Namely, an increase in the potential to -1.3 V also contributes to the more nonuniform and dendritic growth of electrolytic sediment, which is undesirable for the study; the lowest of the proposed potentials was selected for deposition of the samples: -1.1 V.

The XPS data confirms the formation of the aluminum hydroxide phase at the working electrode in the process of electrocrystallization at -1.1 V. An analysis of the Al2p and O1s line profiles has shown the presence of a single Al^{3+} compound (Figure 2). Namely, the presence of the Al_2O_3 phases correspond to binding energies (BE) of 74.40–74.60 eV [18], an oxyhydroxide phase AlOOH to 74.60 eV [19], while the BE of 74.20 eV belongs to $Al(OH)_3$ [20]. The observed Al2p line correlates with the characteristic band for the $Al(OH)_3$ phase precisely. Also, the O1s band matches the BE values for aluminum hydroxide $Al(OH)_3$. The following reaction could take part under the deposition conditions (equation (6)):

$$Al^{3+} + 3OH^- \rightarrow Al(OH)_3 \rightarrow Al_2O_3 + H_2O \quad (6)$$

An XRD analysis was carried out to identify the formation of $Zn(OH)_2$ and $Al(OH)_3$ at the electrodes. It was found that most reflections in diffractograms correspond to $Zn(OH)_2$ (file JCPDS 36-1451) while no reflections of the individual $Al(OH)_3$ phase were found.

All concentrations of metals in the baths were measured experimentally by mass spectrometry (ICP MS). The determined values of the concentrations are fairly close to the corresponding theoretical values, with a margin of error not exceeding 1-5%. The data obtained is given in Table 1 as an atomic percentage × at% Al^{3+} and $(1 - x)$ at% Zn^{2+}.

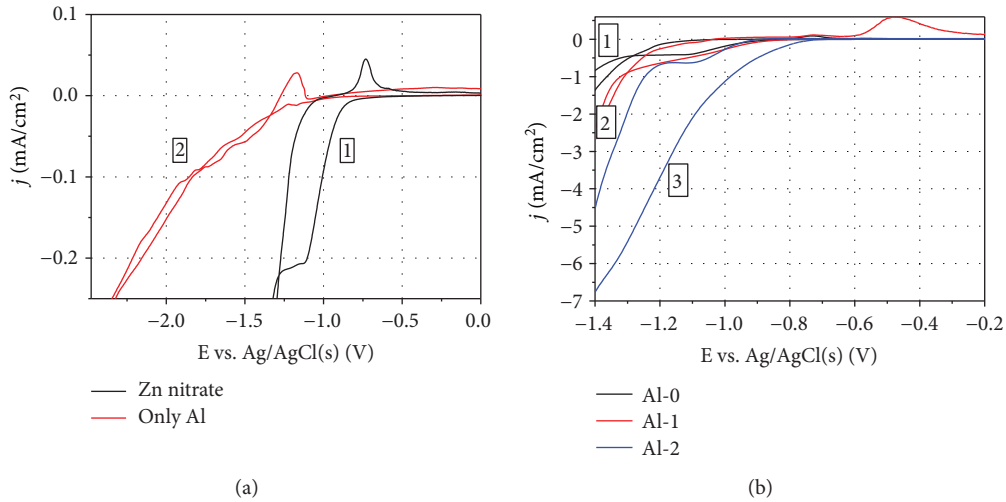

Figure 1: Cyclic voltammograms of ITO electrode in zinc nitrate electrolytes with different concentrations of aluminum nitrate: (a) 1—Al-free zinc nitrate electrolyte and 2—Zn-free aluminum nitrate electrolyte. (b) 1—Al-free electrolyte, 2—1 at.% of aluminum, and 3—2 at.% of aluminum. Scan rate—20 mV/s.

Table 1: Zinc deposition electrolytes and applied deposition methods.

Electrolytes	Electrolyte composition	C(Zn) (ICP MS), mol/l	C(Al) (ICP MS), mol/l	Al/Zn (ICP MS)	Deposition potential, deposition rate
Al-0	0.2 M $Zn(NO_3)_2$ 0.5 M KNO_3				-1.1 V (-1.3 ÷ -1.1 V) vs. Ag/AgCl
Al-1	0.2 M $Zn(NO_3)_2$ 0.5 M KNO_3 0.0032 M $Al(NO_3)_3$	99.02	0.98	0.0099	-1.1 V (-1.3 ÷ -1.1 V) vs. Ag/AgCl
Al-2	0.2 M $Zn(NO_3)_2$ 0.5 M KNO_3 0.0064 M $Al(NO_3)_3$	98.05	1.95	0.0199	-1.1 V (-1.3 ÷ -1.1 V) vs. Ag/AgCl
Al-4	0.2 M $Zn(NO_3)_2$ 0.5 M KNO_3 0.0128 M $Al(NO_3)_3$	96.03	3.97	0.0413	-1.1 V (-1.3 ÷ -1.1 V) vs. Ag/AgCl
Al-6	0.2 M $Zn(NO_3)_2$ 0.5 M KNO_3 0.0192 M $Al(NO_3)_3$	94.00	6.00	0.0638	-1.1 V (-1.3 ÷ -1.1 V) vs. Ag/AgCl
Al-10	0.2 M $Zn(NO_3)_2$ 0.5 M KNO_3 0.0256 M $Al(NO_3)_3$	90.07	9.93	0.1102	-1.1 V (-1.3 ÷ -1.1 V) vs. Ag/AgCl

LAES data for the deposited films show a systematic increase in the aluminum percentage in the bulk of the films which contain much more aluminum than required (Table 2). The characteristic lines of aluminum increased drastically with Al concentration in the electrolytic bath. The dependence of the bulk Al percentage on its concentration in electrolyte can be described by the Langmuir-Freundlich isotherm model for adsorbates as shown in Figure 3.

Table 2 shows the dependence of the experimental atomic fraction of aluminum on its theoretical content in deposited films studied by three independent research methods, such as XPS, EDX, and LAES. Despite significant discrepancies in the data, the averaged values indicate positive deviations in the aluminum content in the samples. So for sample Al-1, the content of aluminum is about 9 at % of dopant (Table 2). For the samples obtained with higher concentrations of dopant in the bath, the mole fraction of aluminum exceeds the calculated values even more significantly, reaching a constant value of about 14.5%.

The EDX data showed a uniform distribution of zinc and aluminum over the surface of the film, but found a complete discrepancy between the ratios of metals in the volume of the films, which is due to the low accuracy of the method

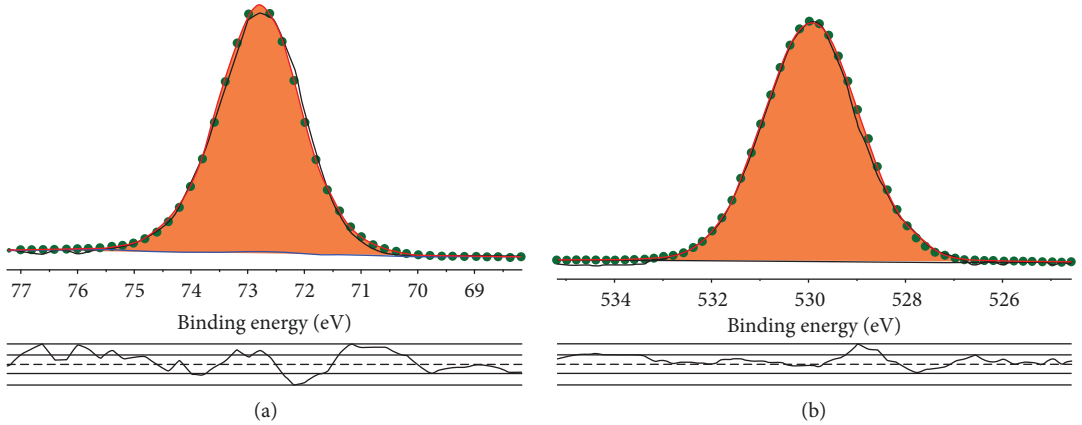

Figure 2: Characteristic XPS bands for Al 2p and O 1s for the sample with theoretical percentage of Al 2 at.%.

Table 2: Characteristics of ZnO:Al coatings after annealing at 530°C for 1 hours. 1 μm thick films have been applied for LAES, EDX, and XPS analyses.

Electrolytes	Zn (LAES), at%	Al (LAES), at%	Al/Zn (LAES)	Zn (EDX), at%	Al (EDX), at%	Al/Zn (EDX)	Zn (XPS), at%	Al (XPS), at%	Al/Zn (XPS)
Al-0		0					34.5	0	0
Al-1	90.9	9.07	0.10	3.03	1.60	0.53	21.0	5.0	0.24
Al-2	86.0	14.0	0.16	2.97	5.59	1.88	7.5	15.0	2.00
Al-4	86.3	13.7	0.16	0.88	1.58	1.80	9.7	7.2	0.74
Al-6	86.0	14.0	0.16	1.63	9.26	5.68	1.3	18.1	13.90
Al-10	84.3	15.7	0.19	3.82	16.13	4.22	23.6	18.9	23.60

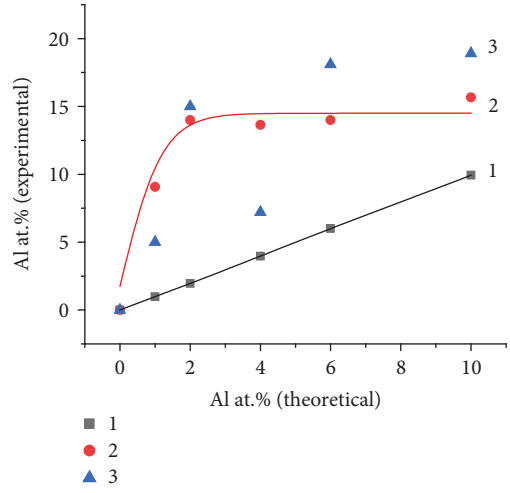

Figure 3: Graphical representation of the Al/Zn ratio in electrolytes and the samples before annealing according to (a) ICP MS data for the electrolytes (1), (b) LAES data (2), and (c) XPS data (3) for 2 μm-thick films with different concentrations of aluminum.

(Table 2). On the other hand, the EDX data confirm the effect of an increased aluminum percentage in the samples that matches LAES data.

A semiquantitative analysis of the surface composition of the films was achieved by XPS spectroscopy. The same effect of the positive deviation of the surface concentration of aluminum was found, and the mole fraction of surface aluminum exceeds its volume percentage. The Al/Zn ratios obtained from the XPS survey spectra are higher than the values found for the bulk of the film by the LAES and EDX methods, which show an integral result for the coating (Figure 3). This result indicates that the composition of the surface of the film probably differs from its bulk.

According to experimental data, the aluminum content on the surface of the film is much higher than the bulk content, as can be seen in Figure 3. The corresponding binding energy peak Al2p could be related to the aluminum hydroxide. The secondary crystallization of the $Al(OH)_3$ phase is typical for all mixed electrolytes. In this case, the percentage of surface aluminum grows with its concentration in the bath and the saturation of the surface occurs if the Al concentration reaches 2 mol.% or even less. So the composition of electrolytes remains below 2 at.% of aluminum, since for the remaining formulations there is an excessive amount of hydroxides on the surface, so in the following optical and electrical experiments the samples with a theoretical dopant percentage of 1 and 2 at.% were studied.

ITO is an appropriate substrate for ZnO crystal growth both in aqueous and alcohol media. As reported by Lebedev et al. [21], a (002)-oriented growth of ZnO nanorods under hydrothermal conditions is observed. The surface morphology of polycrystalline ZnO:Al films deposited at various potentials is always different, including different porosity and particle size. The samples Al-0, Al-1, and Al-2 demonstrate a nonuniformity of thickness, uniform macropores, and sponge-like architecture (Figure 4). An increase in Al

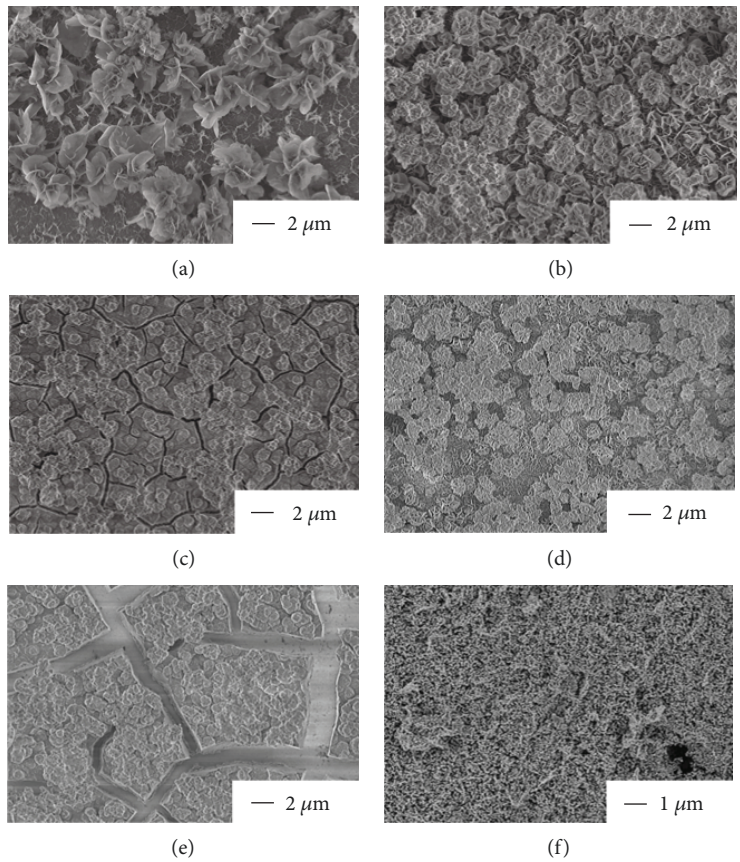

Figure 4: SEM micrographs of ZnO coatings deposited in different aqueous nitrate baths with various Al percentage, namely, (a) ZnO electrolyte, (b) 1 at.% of aluminum, (c) 2 at.% of aluminum, (d) 4 at.% of aluminum, (e) 6 at.% of aluminum, and (f) 10 at.% of aluminum.

percentage in the bulk leads to a much more uniform film growth as seen in Figure 4. However, most uniform films such as Al-6 and Al-10 have shown an excess of $Al(OH)_3$ at the surface according to XPS results. In the following thermal oxidation step, it forms a chemically inert insulator Al_2O_3, which is undesirable for electronic devices.

On the other hand, it is interesting that there are still not many techniques for porous ZnO template synthesis, as porous semiconductive coatings have great potential for different electronic applications including photovoltaics [22]. The formation of pores can be attributed to the enhanced growth height or roughness of the sample and to the hydrogen evolution at the cathode. However, the pores do not alter the structure of ZnO, as it is visible in the image in Figure 4(b), which shows the patterned grains of the sample that are characteristic of the wurtzite structure [22]. The formation of pores in ZnO structures was reported elsewhere.

In the micrographs, it is clear that the grains are thin and flake-like with an average diameter of about 1 μm and thickness of tens of nanometers. The grains are interconnected and uniform and form compact films. The grains of the samples are characterized by the wurtzite structure and indiced as an (110)-oriented flake with a hexagonal zincite-like structure.

In accordance with TG-DTA data (Figure 5), the thermal degradation of pristine deposited coatings above 500°C results in white-color nanocrystalline zinc oxide powders.

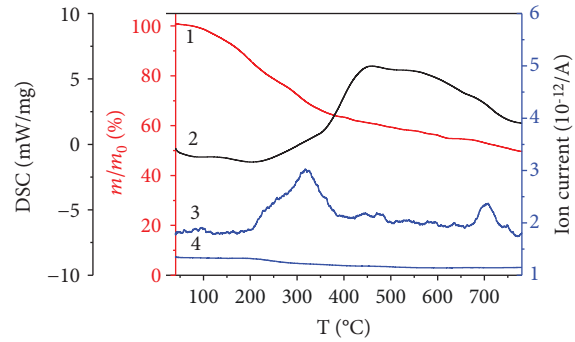

Figure 5: TG-DTA data for pristine ZnO films deposited from nitrate bath at RT before their annealing at 500°C in air. 1—weight loss in w.%, 2—DSC effect, and 3—ICP MS data for releasing gas products with mass numbers of 44 and 18, respectively.

However, a weak CO_2 gas releasing takes place up to 600°C. The films degrade releasing carbon dioxide at 220-300°C and 450-470°C. An additional carbon dioxide release is found above 600°C, likely as a result of the formation of some carbonate in the air. So the obtained deposits can be turned into oxides at 550°C with a further softening of the substrate material.

The electron diffraction (ED) data of individual deposit crystallites also correspond well to the hexagonal ZnO lattice

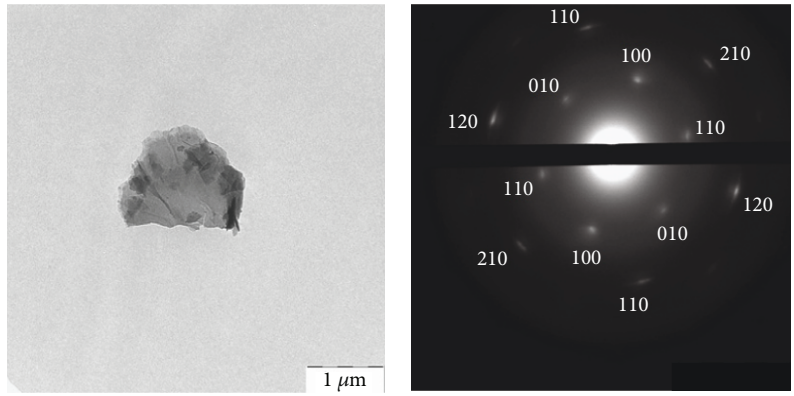

(a) (b)

Figure 6: TEM and electron diffraction data for a single particle of ZnO produced via the annealing process in the Al-0 film.

but not to zinc hydroxide $Zn(OH)_2$. A diffractogram of an individual flat plate-like crystallite is presented in Figure 6.

The transport characteristics of the samples were studied to reveal the formation of an inert Al_2O_3 phase at the surface or ZnO doping by aluminum. The change in the phase composition of the samples during annealing is indicated by the change in the electrical resistivity of the samples, which decreases from (2-4)x106 Ohm·cm approximately by factor 2 for Al-1 - Al-4 samples but not for the Al-6 and Al-10 ones. Generally, the Al doping resulted in the fairly high conductivity of samples. However, insulator admixtures such Al_2O_3 segregate under the annealing conditions onto the ZnO grain boundaries increasing the resistance of the films. Such effect is the most significant for the samples with higher aluminum content.

Also, assuming that the Al/Zn ratio is in an appropriate range, it is expected that during annealing Al^{3+} ions diffuse into the ZnO lattice and some of the Zn^{2+} sites are replaced by Al^{3+}. According to the defect theory, Al^{3+} ion substituted in the crystal lattice acts as an interstitial impurity. At the same time, the electrical conductivity of AZO films depends on the oxygen vacancy and the contribution of Zn − Al interstitial atoms. The drop in oxygen vacancies reduces the concentration of carriers, thereby increasing resistivity.

3.2. Optical Characteristics. Al-doped ZnO films were studied by optical spectroscopy in the UV-vis range to characterize their optical transparency and reflectance inputs. Figure 7 demonstrates the direct (regular) transmittance spectra of ZnO deposited on ITO substrates from an aqueous nitrate electrolyte. The theoretical thickness of the deposited films varied from 1000 to 2000 nm to reach the full coating of the ITO glass and also to reveal the samples with the finest optical and structural characteristics.

Both undoped and Al-doped films have strong absorption in the UV region and good transmittance of 75% in the visible region. The absorption intensity of Al-doped films increases slowly in the visible range, and the absorption peaks are not obvious in comparison with undoped ZnO where the absorption intensities increase rapidly at the absorption edge. This means that Al doping degrades the film crystal quality.

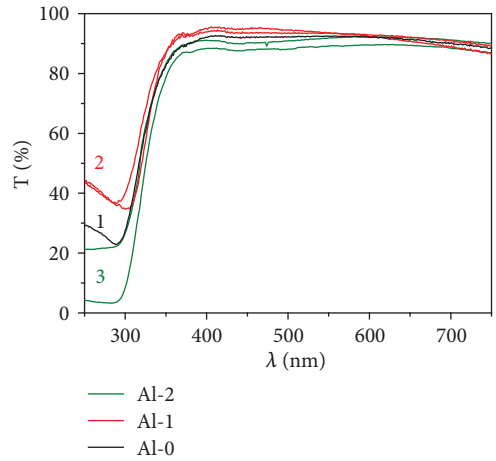

Figure 7: Optical transmittance spectra of ZnO coatings of 1—Al-0, 2—Al-1, and 3—Al-2 with different thicknesses of 1000 nm and 2000 nm.

Otherwise, Al doping leads to a slight blue shift of the film absorption edge and the shift increases monotonically with an increase in Al concentration as reported by [6]. Most likely, this shift originates from surface Al_2O_3 but also corresponds to the Burstein-Moss effect [10]. The blue shift behavior in the band gap can be attributed to an increase in the carrier concentration that blocks the lowest states in the conduction band, known as the Burstein–Moss effect. Such an increase in the carrier concentration in Al-doped ZnO will cause the Fermi level to move into the conduction band.

The ion Al^{3+} radius is smaller than that of Zn^{2+}. The substitution of lattice Zn^{2+} with Al^{3+} would widen the ZnO bandgap. The blue shift of the absorption edge of the doped films indicates that the doped Al^{3+} ions are located in the lattice site forming $Zn_{1-x}Al_xO$ alloys. The profiles of the transmittance spectra correlate well with the spectra reported in Ref. [10].

Photoluminescence data is shown in Figure 8. Since only electrolytes with a low aluminum content are of practical importance, we consider samples with 0 or 1 at % Al as Al-substituted samples. The low luminescence intensity for the

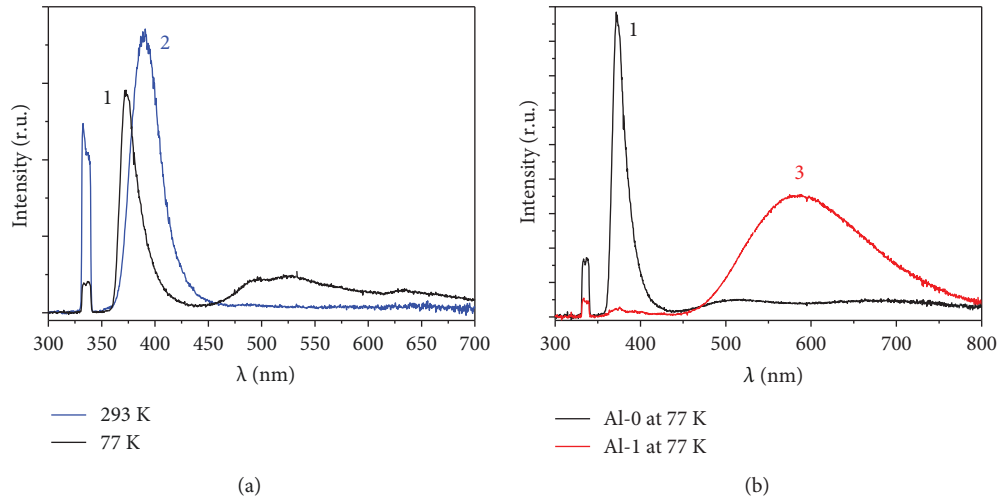

FIGURE 8: Photoluminescence spectra of ZnO:Al coatings deposited from zinc-aluminum nitrate electrolytes. (a) PL spectra for Al-0 (Al-free) films at 1—77 K and 2—293 K. (b) The PL spectra of 1—Al-0 and 3—Al-1 (1 at.% of Al (theoretical)) collected at 77 K. The excitation wavelength of 337 nm.

doped sample, the maximum in the visible region, indicates a low defect in the crystallites. Room-temperature PL spectra show a strong UV emission and an improved UV-to-visible emission ratio, a clear indication for high optical quality ZnO films.

The near-band-edge luminescence (NBE) of crystalline ZnO was collected at 77 K and 293 K, and there are only strong lines in the spectra at 370 nm (3.35 eV) and 395 nm (3.14 eV) correspondingly. In the PL spectrum collected at 77 K both green and yellow lines of intrinsic defects, Zn_i'' and $V_O^{\cdot\cdot}$ were observed as week bands.

In the PL spectra of the samples with the lowest theoretical percentage of aluminum of 1 at.%, a strong maximum at 600 ± 80 nm (2.07 ± 0.31 eV) is observed at 77 K. The large peak width corresponds, most likely, to a mixed input of different defects including the yellow line of oxygen vacancies $V_O^{\cdot\cdot}$ (550 nm or 2.25 eV) or interstitial atoms [6, 21, 23]. According to Ref. [24] various Al_{Zn}–O_i complexes make a strong input to the yellow band at 550 nm. At the same time, the NBE bands of the Al-1 sample show a slight blue shift for doped samples moving the NBE to 370 nm (3.35 eV) [25].

For the comparison, all samples with higher theoretical percentage of aluminum (with Al-reached surfaces) showed a different character of their PL spectra. These spectra included the blue shoulder right near the NBE bands at 440 ± 450 nm (2.76 eV) and a broad maxima in the red region at 700 ± 100 nm (1.77 ± 0.30 eV). These lines were not observed in the spectrum of the Al-1 sample. They could be also related to AZO point defects ($V_O^{\cdot}$, Zn_i', and O_i'', correspondingly) [24], but, most likely, they are associated with unknown defects in crystalline alumina.

4. Conclusions

The samples obtained in the zinc-aluminum nitrate aqueous electrolyte are, most likely, doped ZnO:Al or ZnO:Al with some Al_2O_3 admixture at the surface. An important advantage of this electrolyte composition is the intensive oxidation of the electrolytic precipitate. No metal phase has been detected in the samples which means ZnO films can be obtained from nitrate electrolyte in a single step, without any additional oxidants. Also, a positive deviation in the aluminum percentage in the sample could be reduced if electrolytes are used with a smaller concentration of the dopant. The doping of ZnO with Al has produced a new photoluminescence maximum originated from different kinds of point defects as oxygen vacancies are included both as a substitute for Zn by Al^{3+} ions in the ZnO lattice with coordinated interstitial oxygen.

On the other hand, the microstructure of the films is porous, which is appropriate for semiconductive scaffolds for solar cells but less suitable for most TCO layers in microelectronics. Subsequent studies should focus on improving this deposition technique.

Data Availability

The data used to support the findings of this study are obtained by all authors at Lomonosov Moscow State University (MSU), Lebedev Physical Institute (LPI) of the Russian Academy of Sciences, Prokhorov General Physics Institute of the Russian Academy of Sciences (GPI), and ZAO "SPECS". The composition characterization data (ED, XRD, XPS, and TG-DTA MS data) used to support the findings of this study are included within the article. The SEM data used to support the findings of this study are included within the scope of the article. The diffuse spectroscopy data are performed in MSU and used to support the findings of this study which are included within the article. The photoluminescence spectroscopy data carried out in LPI and used to support the findings of this study are included within the article. The twofold resistance measurements are carried out in GPI using an original setup. LAES measurements are obtained using an original setup developed by ZAO "SPECS".

Disclosure

The project was performed using the equipment and setups of the collective resource center of Moscow State University "Technologies for synthesis of new nanostructured materials and their complex characterization."

Conflicts of Interest

The authors declare that they have no conflicts of interest.

Acknowledgments

Authors are grateful to colleagues from Moscow State University for their assistance in experiments, namely, Prof. Andrei V. Shevelkov, Prof. Alexander V. Knotko, Dr. Olga V. Boytsova, Dr. Tatyana Shatalova, Dr. Sergey S. Abramchuk, and Prof. Eugene Goodilin. This work is supported by the Russian Foundation for Basic Research (grant 19-03-00849_a).

References

[1] G. G. Valle, P. Hammer, S. H. Pulcinelli, and C. V. Santilli, "Transparent and conductive ZnO:Al thin films prepared by sol-gel dip-coating," *Journal of the European Ceramic Society*, vol. 24, no. 6, pp. 1009–1013, 2004.

[2] S. Yoshioka, F. Oba, R. Huang, I. Tanaka, T. Mizoguchi, and T. Yamamoto, "Atomic structures of supersaturated ZnO–Al_2O_3 solid solutions," *Journal of Applied Physics*, vol. 103, no. 1, article 014309, 2008.

[3] M. Maache, T. Devers, and A. Chala, "Al-doped and pure ZnO thin films elaborated by sol-gel spin coating process for opto-electronic applications," *Журнал технической физики*, vol. 51, no. 12, pp. 1663–1668, 2017.

[4] J. W. Elam and S. M. George, "Growth of ZnO/Al_2O_3 alloy films using atomic layer deposition techniques," *Chemistry of Materials*, vol. 15, no. 4, pp. 1020–1028, 2003.

[5] J. Han, P. Q. Mantas, and A. M. R. Senos, "Densification and grain growth of Al-doped ZnO," *Journal of Materials Research*, vol. 16, no. 2, pp. 459–468, 2001.

[6] E. Shkondin, O. Takayama, M. E. A. Panah et al., "Large-scale high aspect ratio Al-doped ZnO nanopillars arrays as anisotropic metamaterials," *Optical Materials Express*, vol. 7, no. 5, p. 1606, 2017.

[7] C. Gümüş, O. M. Ozkendir, H. Kavak, and Y. Ufuktepe, "Structural and optical properties of zinc oxide thin films prepared by spray pyrolysis method," *Journal of Optoelectronics and Advanced Materials*, vol. 8, pp. 299–303, 2006.

[8] R. Groenen, J. Löffler, P. M. Sommeling et al., "Surface textured ZnO films for thin film solar cell applications by expanding thermal plasma CVD," *Thin Solid Films*, vol. 392, no. 2, pp. 226–230, 2001.

[9] D. Herrmann, M. Oertel, R. Menner, and M. Powalla, "Analysis of relevant plasma parameters for ZnO:Al film deposition based on data from reactive and non-reactive DC magnetron sputtering," *Surface and Coatings Technology*, vol. 174-175, pp. 229–234, 2003.

[10] M. Zubkins, R. Kalendarev, K. Vilnis, A. Azens, and J. Purans, "Structural, electrical and optical characteristics of Al-doped zinc oxide thin films deposited by reactive magnetron sputtering," *IOP Conference Series: Materials Science and Engineering*, vol. 49, article 012057, 2013.

[11] Z. Y. Ning, S. H. Cheng, S. B. Ge et al., "Preparation and characterization of ZnO:Al films by pulsed laser deposition," *Thin Solid Films*, vol. 307, no. 1-2, pp. 50–53, 1997.

[12] J. Weng, Y. Zhang, G. Han et al., "Electrochemical deposition and characterization of wide band semiconductor ZnO thin film," *Thin Solid Films*, vol. 478, no. 1–2, pp. 25–29, 2005.

[13] D. Ramírez, D. Silva, H. Gómez, G. Riveros, R. E. Marotti, and E. A. Dalchiele, "Electrodeposition of ZnO thin films by using molecular oxygen and hydrogen peroxide as oxygen precursors: structural and optical properties," *Solar Energy Materials and Solar Cells*, vol. 91, no. 15–16, pp. 1458–1461, 2007.

[14] G. Riveros, D. Ramírez, A. Tello, R. Schrebler, R. Henríquez, and H. Gómez, "Electrodeposition of ZnO from DMSO solution: influence of anion nature and its concentration in the nucleation and growth mechanisms," *Journal of the Brazilian Chemical Society*, vol. 23, no. 3, pp. 505–512, 2012.

[15] M. Wang and X. Wang, "Electrodeposition zinc-oxide inverse opal and its application in hybrid photovoltaics," *Solar Energy Materials and Solar Cells*, vol. 92, no. 3, pp. 357–362, 2008.

[16] Q. Hou, F. Meng, and J. Sun, "Electrical and optical properties of Al-doped ZnO and $ZnAl_2O_4$ films prepared by atomic layer deposition," *Nanoscale Research Letters*, vol. 8, no. 1, pp. 144–149, 2013.

[17] A. Peić, T. Dimopoulos, R. Resel et al., "Effect of AZO substrates on self-seeded electrochemical growth of vertically aligned ZnO nanorod arrays and their optical properties," *Journal of Nanomaterials*, vol. 2012, Article ID 457904, 14 pages, 2012.

[18] P. H. Bolt, E. Ten Grotenhuis, J. W. Geus, and F. H. P. M. Habraken, "The interaction of thin NiO layers with single crystalline α-Al_2O_3(1120) substrates," *Surface Science*, vol. 329, no. 3, pp. 227–240, 1995.

[19] H. He, K. Alberti, T. L. Barr, and J. Klinowski, "ESCA studies of aluminophosphate molecular sieves," *The Journal of Physical Chemistry*, vol. 97, no. 51, pp. 13703–13707, 1993.

[20] A. Hess, E. Kemnitz, A. Lippitz, W. E. S. Unger, and D.-H. Menz, "ESCA, XRD, and IR characterization of aluminum oxide, hydroxyfluoride, and fluoride surfaces in correlation with their catalytic activity in heterogeneous halogen exchange reactions," *Journal of Catalysis*, vol. 148, no. 1, pp. 270–280, 1994.

[21] V. A. Lebedev, A. I. Gavrilov, A. S. Shaporev, V. K. Ivanov, B. R. Churagulov, and Y. D. Tret'yakov, "Hydrothermal and hydrothermal-microwave syntheses of oriented nanorods of zinc oxide on an ITO substrate," *Doklady Chemistry*, vol. 444, no. 1, pp. 117–119, 2012.

[22] Z. Liu, Z. Jin, J. Qiu, X. Liu, W. Wu, and W. Li, "Preparation and characteristics of ordered porous ZnO films by a electrodeposition method using PS array templates," *Semiconductor Science and Technology*, vol. 21, no. 1, pp. 60–66, 2006.

[23] O. A. Shalygina, I. V. Nazarov, A. V. Baranov, and V. Y. Timoshenko, "Structure and photoluminescence properties of zinc oxide/ytterbium oxide nanocomposites," *Journal of Sol-Gel Science and Technology*, vol. 81, no. 2, pp. 333–337, 2017.

[24] J. Lv, C. Li, and J. J. BelBruno, "Characteristics of point defects on the optical properties of ZnO: revealed by Al–H co-doping and post-annealing," *RSC Advances*, vol. 3, no. 23, pp. 8652–8656, 2013.

[25] H. Rotella, Y. Mazel, S. Brochen et al., "Role of vacancy defects in Al doped ZnO thin films for optoelectronic devices," *Journal of Physics D: Applied Physics*, vol. 50, no. 48, article 485106, 2017.